Surface & Coatings Technology 364 (2019) 377–382

Contents lists available at ScienceDirect

Surface & Coatings Technology

journal homepage: www.elsevier.com/locate/surfcoat

A new approach to characterize charge transfer reaction for solid oxide fuel cell

Sanghoon Lee[a], Taehyun Park[b], Wonyeop Jeong[a], Inwon Choi[a], Hyung Gyu Park[c], Arunkumar Pandiyan[a,d], Suresh Babu Krishna Moorthy[d], Ikwhang Chang[e,*], Suk Won Cha[a,*]

[a] Department of Mechanical and Aerospace Engineering, Seoul National University, 1, Gwanak-ro, Gwanak-gu, Seoul 08826, Republic of Korea
[b] Department of Mechanical Engineering, Soongsil University, Sangdo-ro 369, Dongjak-gu, Seoul 06978, Republic of Korea
[c] Nanoscience for Energy Technology and Sustainability, Department of Mechanical and Process Engineering, Eidgenössische Technische Hochschule (ETH) Zürich, Tannenstrasse 3, CH-8092 Zürich, Switzerland
[d] Centre for Nanoscience and Technology, Madanjeet School of Green Energy Technology, Pondicherry University, Puducherry 605 014, India
[e] Department of Automotive Engineering, Wonkwang University, 460 Iksan-daero, Iksan, Jeonbuk 54538, Republic of Korea

ARTICLE INFO

Keywords:
Solid oxide fuel cell
Patterned electrode
Thin film
Pt cathode
Reactive ion etch
Charge transfer reaction

ABSTRACT

We developed a novel approach to characterize the electrochemical reaction of solid oxide fuel cell. The method constrained electrode-electrolyte interface geometry and thereby limited reaction area for charge transfer. Reactive ion etch (RIE) and sputtering techniques were used and the well-defined geometry of interfaces was realized as patterned strips. The number of strips of the pattern shape was fully consistent with the value of charge transfer impedance. The confined interface structure also helped maintain open circuit voltage for 10 h. This new approach proposes an alternative to quantitatively analyze different electrode materials for SOFC operation while excluding consideration for structural variables.

1. Introduction

One of the fuel cells' prime advantages is that it converts the chemical energy of fuels directly into usable electrical energy. As a result, fuel cells exhibit much higher efficiency unlike other energy conversion devices going through multiple conversion steps. The direct energy conversion in fuel cells occurs at triple phase boundaries, so-called TPBs where fuels, electrodes, and electrolytes meet simultaneously [1,2]. Therefore, augmenting domains of TPBs leads to an enlargement of the reaction zone, which is directly linked to the decrease in activation loss.

A large number of researches have been done to enlarge TPBs for solid oxide fuel cells (SOFCs) using various fabrication processes [3–7]. Especially adoption of thin film processes for the fabrication of SOFC component is noteworthy [8–11]. Those processes substantially expand the surface area of the electrode-electrolyte interface and enable controlling the TPBs in nanoscale, creating much more reaction zones and hence increase the performances. Diverse nano-/micro-structures have been demonstrated including core-shell, porous thin films, or corrugated structure [10–15].

Although nano-/micro-fabrication methods have been developed recently, these geometries are still produced from conventional SOFC fabricating processes like screen printing or tape casting [16,17]. Reproducibility of the microstructure is crucial here. By adjusting the process parameters, the nano-/micro-structures of electrode-electrolyte electrochemical interface change due to various process environment [5,7]. As long as the SOFCs' elements are formed in a specific process parameter, the components created with the same parameters are assumed to share the identical nano-/micro-structures with each other. This assumption affects the analysis of SOFCs. However, those typical processes do not produce 100% same nano-/micro-structures even though the process parameters are exactly the same. In other words, SOFCs produced by the conventional processes are lack of reproducibility, especially in nanoscale. Therefore, even if different SOFCs produced with same parameters were characterized based on a supposition that they both have the same geometries, the cells may not show the same electrochemical behavior. Comparison of SOFCs with different materials has low reliability in this sense because the structural factor cannot be completely eliminated.

A number of researches on confined electrode structure have been studied [18–20]. Chueh et al. reported that the reasons for enhancement in electrocatalysis from thin film SOFCs (TF SOFCs) with porous electrode structure are unclear [20]. Unequivocal assessment of the subject can be hardly made, such as, whether the performance change shown is from increased metal phase interconnection, or extended

* Corresponding authors.
E-mail addresses: ikwhang2@wku.ac.kr (I. Chang), swcha@snu.ac.kr (S.W. Cha).

https://doi.org/10.1016/j.surfcoat.2019.01.083
Received 31 August 2018; Received in revised form 9 January 2019; Accepted 23 January 2019
Available online 25 January 2019

TPBs, or improved interfacial property.

In this study, a novel method to electrochemically characterize cathode materials is proposed, through a confined reaction area with constrained electrode-electrolyte interface. Specifically, a response of charge transfer reaction was investigated through a cathode consisted of a number of embedded Pt strips using electrochemical impedance spectroscopy (EIS). The dense thin film Pt cathode was deposited on the trenched area on the electrolyte, constituting the embedded Pt strip. This forms extremely confined electrode-electrolyte interface and realizes TPBs existing only on the perimeter of the strips. Thereby, adjusting the number of strips can virtually linearly control the domain of reaction sites of the cathode. As far as the authors' knowledge, this is the first work that reports trench-structured electrode-electrolyte interface compared to reported literature with artificially confined electrode-electrolyte geometry. The trench-structured interface will more firmly confine the electrode within the “ditch space” of electrolyte from thermal impact during SOFC operation than electrode strips simply laid on electrolyte surface. The well-defined electrode geometry was fabricated with reactive ion etching (RIE) and direct current (DC) magnetron sputtering of Pt on single crystal (100) yttria-stabilized zirconia (YSZ) pellet. Through the electrode with crafted geometry, the SOFC showed a clear correlation between electrochemical behavior and the model electrodes.

2. Experimental

Fig. 1 shows the overall fabrication process for the SOFC with engraved Pt strips cathode. A commercial single crystal (100) YSZ pellet ($1 \times 1\ cm^2$) was coated with NiO-YSZ via a screen printing method using a commercial NiO-YSZ (50:50) solution ink. The anode was coated on the whole pellet area and the pellet was sintered at 1300 °C for 3 h, followed by reducing. The reduction was carried out at 750 °C with 100 sccm of pure H_2 gas flow for 5 h. After reduction, the pellet was then loaded on a substrate which can be clamped with a lid. The lid has 9 mm × 9 mm openings for modification of sample surface and a patterned shadow mask was laid between the pellet and the lid so that the clamped lid can pressurize the mask enough. The patterned shadow mask has patterned 5 mm long strips with a width of 100 μm. The patterns have 200 μm and 400 μm space between each strip for 20 strips pattern and 12 strips pattern, respectively. For 5 strips pattern, Kapton tape was attached to block 7 strips out of the 12 strips pattern, so that only 5 strips are to be exposed. The cells with the mask on it then went through a reactive ion etch (RIE) process. RIE was processed for 2 h and reactant gas was BCl_3. The BCl_3 gas was injected into the chamber with 20 sccm flow rate and chamber atmosphere was maintained to be 20 mTorr. The DC plasma power for etching reached 200 W. After RIE, the cells on the substrate went to the sputter chamber intact and underwent the cathode deposition process via sputtering. The Pt cathode was sputtered using DC magnetron sputtering with DC power of 200 W at room temperature. Ar gas filled the sputtering chamber at a pressure of 5 mTorr. The fabricated SOFC with the patterned electrode was characterized electrochemically and visibly. Electrochemical characterization was done with electrochemical impedance spectroscopy (EIS). The fuel during the electrochemical test was 3% humidified H_2 gas and the flow rate was 100 sccm. The cathode was exposed to ambient air at the operating temperature of 500 °C. EIS scanned the electrochemical response of the cell with a frequency range from 10^6 Hz to 2 Hz. Atomic force microscopy (AFM, PSIA XE150, Park systems, South Korea) was utilized to investigate the microscale geometry of the pattern strips and the samples were scanned with the non-contact mode of the AFM tip. Detailed pre- and post-operation morphology and grain structure were observed through field emission scanning electron microscopy (FESEM, Supra 40, Carl Zeiss, Germany) with 2 kV of operating voltage. Energy Dispersive X-ray Spectroscopy (EDS) was utilized to observe elemental distribution around the strip electrode and it was conducted with the same FESEM equipment.

3. Results and discussion

Fig. 2 shows schematic (a), (c), and (e) and optical images (b), (d), and (f) of the fabricated SOFCs with the patterned electrode. In order to compare the polarization resistance of the electrodes with the different number of strips, flawless geometry of the patterns must be secured. For further investigation on completeness of pattern generation, the patterned structure was observed by FESEM, AFM, and EDS.

As shown in Fig. 3(a), a dimension of each strip was 100-μm-thick width while the width of the as-etched strip was 94-μm-thick. The value of the width is slightly different with the designed value, showing a 6% difference in width. Although RIE involves chemical etch process, physical etch through ion bombardment also takes place during the etching process [21]. The slight discrepancy, between the width of the as-etched strip and the designed strip, is attributed to the shadowing effect in which the indent angle of ion bombardment was not perpendicular to the physical mask [22]. It is also verified in Fig. 3(c), which shows a line profile of the surface of the as-etched (Fig. 3(b)) and as-deposited (Fig. 3(d)) samples. The location of the dotted lines in Fig. 3(b) and (d) was chosen to represent the neutral surface of each sample, not to include too high bumps (expressed as extremely bright color). The line profile of the as-etched pellet (black line) drops gradually with a slope. Not only the width of the as-etched strip became smaller, but also etched line profile did not form a sharp step. In addition, at the boundary of the electrolyte-electrode interface (around 30–50 μm of the x-axis in Fig. 3(c)), the line profile rose up for about ~100 nm for both as-deposited and as-etched sample. Those bumps are possibly derived from two factors: (1) redundant residues or chips as a result of RIE or (2) an equipment-driven error, an overshoot error due

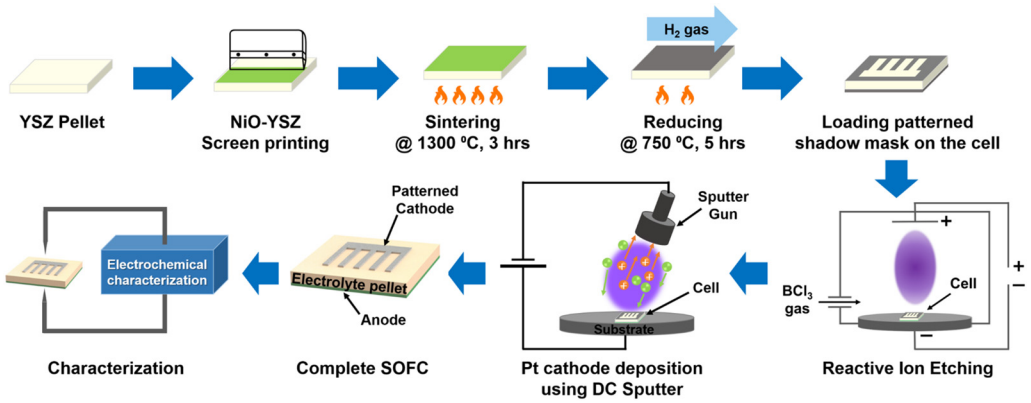

Fig. 1. Schematic of fabrication process for the solid oxide fuel cell with patterned cathode.

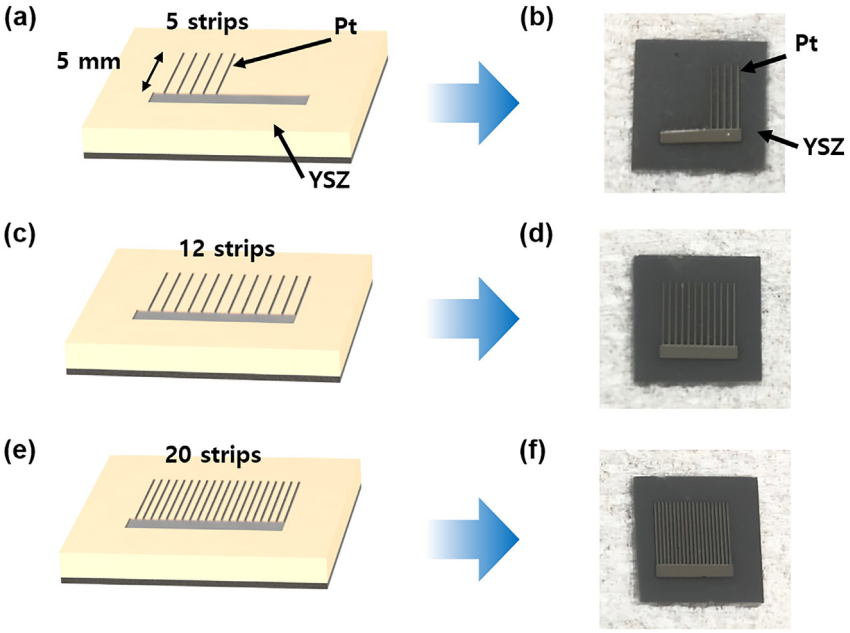

Fig. 2. A schematic illustration of SOFC with patterned (a) 5 strips cathode, (c) 12 strips cathode, and (e) 20 strips cathode and (b) an optical image of the cell with 5 strips cathode, (d) 12 strips cathode, and (f) 20 strips cathode.

to over-lifted or less-pushed down AFM probe passing by sharp topographical steps [23]. Post-process to remove residues after RIE was not carried out to preserve etched pattern geometry. The bare condition of pellets after RIE thus has some residues or chips at the interface. In addition to the second factor, the smooth line profile of the as-etched sample surface may also be stem from the non-contact mode operation of the AFM tip. It would exhibit low nanoscale resolution considering it scanned about 70 μm sized squares.

The single crystal YSZ pellet was etched for about 550 nm. Pt cathode was deposited in the etched space right after the RIE process, which took up to 200 nm. As a result, the depth of the as-deposited trenched electrode reached ~350 nm. The hatched area between the plots in Fig. 3(c) indicates the region where the thin film platinum electrode deposited. The trenched electrode has extremely dense morphology. Morphology of sputtered thin films highly depends on the topography and properties of a base substrate as well as deposition conditions [24–26]. The Ar background pressure of 5 mTorr during the magnetron sputtering process combined with the smooth and dense YSZ pellet yielded exceedingly packed morphology of the sputtered Pt electrode. The trenched electrode thus created reaction sites only on the perimeter of the pattern strips where the electrolyte and catalyst meet. Fig. 3(f) helps to visualize the reaction sites placement. Note that relatively high distribution of Y and Zr on the strip region compared to Pt on out-of-strip region is due to electron beam penetration depth ranged from hundreds of nm to several μm. It is clearly visualized that the reaction sites where electrolyte and electrode meet formed only on the perimeter of the strips. Thereby, the domain of reaction sites would be linearly proportional to the number of strips and patterned electrodes. The cells with the different number of strips would show a discrepancy in polarization resistance.

Electrochemical characterization results are shown in Fig. 4. The electrochemical test was carried out at a temperature of 500 °C and bias of 1.0 V. 100 sccm of 3% hydrated Hydrogen gas was supplied on the fuel electrode side while cathode was exposed to ambient air. Fig. 4(a) is EIS Nyquist plot of the SOFCs with patterned electrodes while the black one, blue one, and red one each represents EIS data of the SOFCs

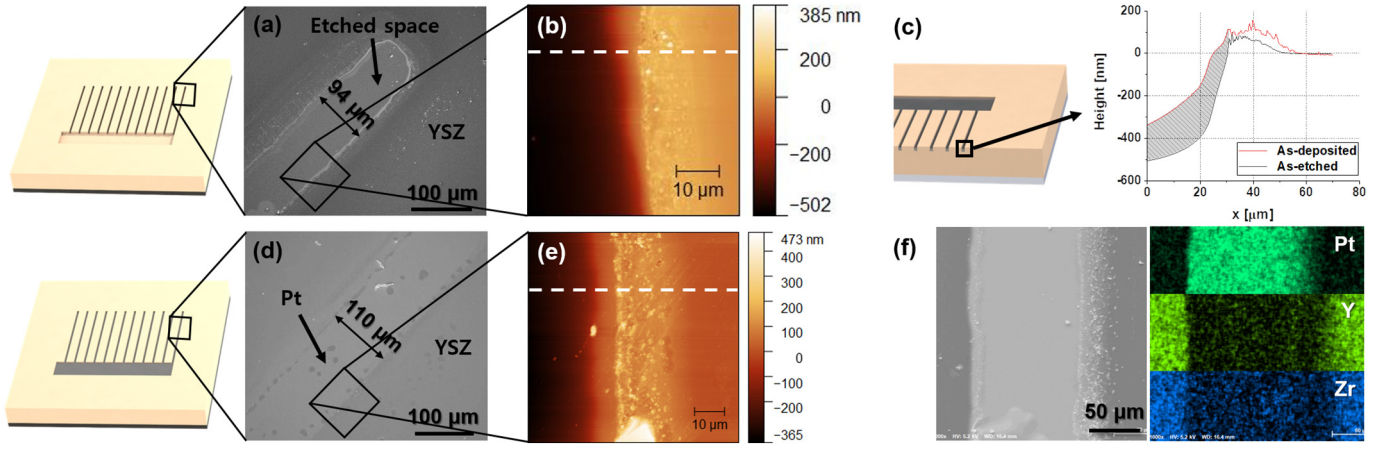

Fig. 3. FE-SEM image and AFM scanned image of the surface of as-etched YSZ pellet ((a), (b)) and those of the surface of as-deposited Pt cathode ((d), (e)) respectively. The dotted lines in (b) and (e) indicate the location where line profiles of (c) were extracted. (c) Line profile of as-etched and as-deposited samples and hatched area between each indicates deposited platinum electrode. (f) EDS analysis of the middle of the patterned electrode. (Left) FESEM image of the mapped electrode strip and (Right) EDS analysis (same area to (Left)) with areal elemental mapping of the Pt|Y|Zr.

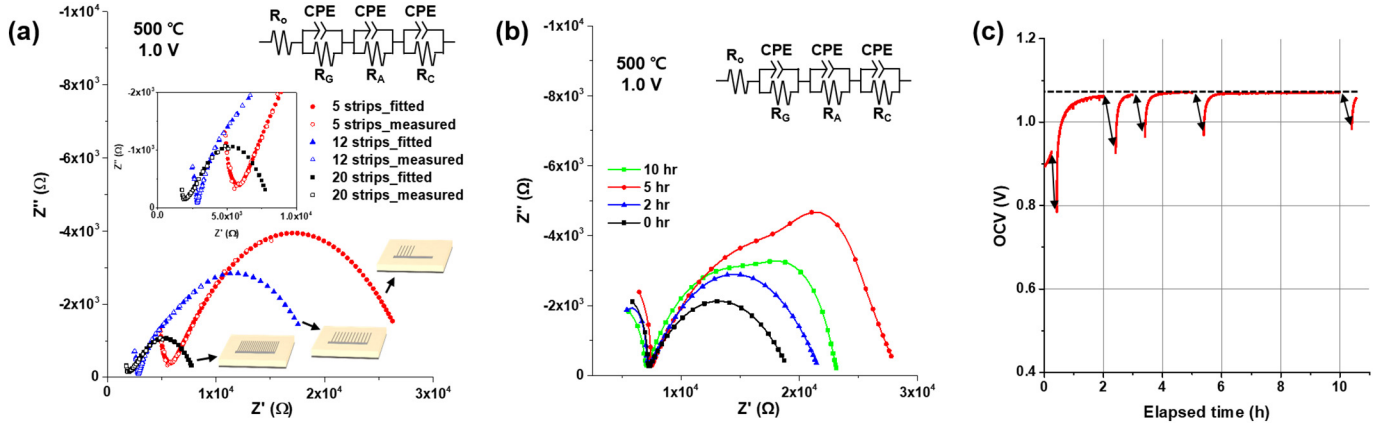

Fig. 4. Electrochemical characterization of the SOFCs with the patterned electrode. (a) EIS Nyquist plot of the model SOFCs with three kind of pattern structures, measured at the 1.0 V bias and 500 °C (○: measured data, ●: fitted and simulated data), (b) time evolution of the measured EIS Nyquist plot from when the cell reached 500 °C, (c) time evolution of open circuit voltage (intermittently disconnected OCV curve, pointed by black arrows, is due to EIS measurement).

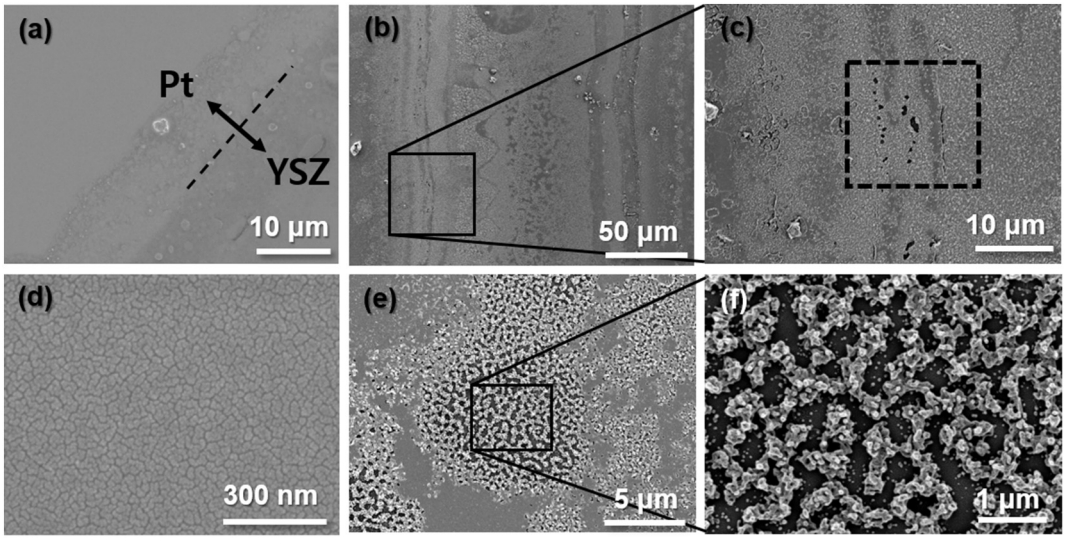

Fig. 5. FESEM surface image of (a), (d) as-deposited Pt cathode and (b), (c), (e), (f) Pt cathode after 10 h of operation. Image of (a) the interface of Pt cathode and YSZ electrolyte and (d) enlarged Pt surface before the operation. Surface image of (b) Pt strip after 10 h of operation, (c) enlarged image of the squared area in (b) (the dotted square indicates delaminated part). Surface image of (e) delaminated part of the Pt cathode, and (f) enlarged image of the squared area in (e).

with 20 strips patterned cathode (20 strips cell), the SOFC with 12 strips patterned cathode (12 strips cell), and the SOFC with 5 strips patterned cathode (5 strips cell) respectively. The impedance value was not electrode-area normalized here, i.e., not area specified, in order to compare the values of resistance based on reaction area variation. Because of the highly limited reaction area at the cathode, the EIS plot reached a very high value, tens of thousands ohms. As can be observed in Fig. 5(a) and (d), as-deposited Pt cathode shows highly dense morphology and it thus resulted in confined reaction sites distribution, only on the perimeter of the strips. Here, the Ni-YSZ cermet anode with porous and tens of micrometer thickness was considered to have minimal impact on polarization resistance. Therefore, major differences in those Nyquist plots are believed to be largely originated from the patterned Pt at the cathode. The measured EIS Nyquist plots of each cell were fitted and simulated based on original experimental data to make arcs for the sake of simplified comparison. The simulated equivalent circuit model is illustrated in the plots. The model includes components for ohmic resistance and charge transfer component for anode and cathode, as well as an effect of the grain boundary. In Fig. 4(a), at the first sight, the size of three distinctive half circle looks certainly different. The different number of strips yielded the difference in reaction area and thereby produced each distinctive Nyquist plot. The faradaic impedance is known as a diameter of half circle of Nyquist plot. The 20 strips cell showed the faradaic impedance value of about 5724 Ω (black colored) while the faradaic resistance of the 12 strips cell exhibited 14,688 Ω (blue colored). The largest value among three is from the 5 strips cell, 20,500 Ω (red colored). The ratio of the faradaic impedance of those three cells is 1:2.56:3.58 (= 5724:14,688:20,500). This ratio is precisely consistent with a ratio of the number of strips for each pattern, which is 1:2.4:4 (= 5:12:20). Furthermore, the ratio of the faradaic resistance of those cells is exactly in inverse proportion to the TPB density ratio of each, which was measured to be 16.7 cm^{-1} for 5 strips cell, 40 cm^{-1} for 12 strips cell and 66.7 cm^{-1} for 20 strips cell, respectively. The density of TPB was calculated as a reciprocal of the half of the sum of the strip width and the distance between strips, which was also used in the characterization of SOFC with the patterned electrode by Haile group [20,27]. On the other hand, the ohmic resistance which is the first x-axis intercept of the Nyquist plots displayed slightly different value for each cell. The structure of pattern strips caused the difference of ohmic resistance. As the number of strips increased, the ohmic resistance decreased. This is obvious, considering that resistance is inverse proportional to electrode area from Ohm's law. The ohmic impedance values are 2040 Ω, 2870 Ω, and 5754 Ω for 20 strips cell, 12 strips cell, and 5 strips cell respectively. The direct judgment of ohmic

impedance based on the number of Pt strips would possess many flaws since ohmic impedance includes not only current collection resistance within electrode but also electrolyte ohmic loss, current collection loss passing through connected parts between the cell and outer circuits, etc.

The confined electrode-electrolyte geometry contributed to relatively stable long-term operation as well. Pure platinum electrode does not show a decent stable long-term operation in general even after an hour operation at 500 °C [11,28]. Agglomeration of Pt grains occur in that temperature and enlarged grains have fewer TPB sites. It eventually leads to increase of the faradaic impedance or even sharp fall of open circuit voltage. The increase of faradaic resistance as the time flows happens in this cell as well. Fig. 4(b) represents the EIS Nyquist plot variation of the patterned SOFC over time for 10 h of operation. Until the cell had operated for 5 h, the faradaic resistance of the cell kept increasing. The increase of the faradaic impedance is attributed to the Pt grain agglomeration at 500 °C. Pt is known to be thermally unstable even at 500 °C. Notably, around the perimeter of the cathode strips, the agglomerated grains resulted in a lower surface area of the catalyst. Accordingly, the reaction area shrank and the faradaic resistance increased. However, Nyquist plot of the cell at 10 h exhibited lower faradaic resistance value than that of the cell at 5 h. Delamination of the platinum thin film is considered to be the cause for the shrinkage of faradaic resistance at 10 h. 10 h of operation at 500 °C is a significantly harsh condition for Pt electrode microstructure stability. Continuous agglomeration of Pt keeps drawing surrounding grains. Few hundreds of nanometer Pt thin film can all be drained and eventually the YSZ electrolyte pellet would be exposed. The delaminated Pt thin film formed the porous structure as shown in Fig. 5(c), (e), and (f). It created quite a plenty of new TPBs, leading to an increased reaction rate. Although delamination of Pt aroused decrease of faradaic impedance after 10 h of operation, the open circuit voltage kept staying at 1.067 V. Intermittent measurement of EIS made the OCV of the cell drop. However, it steadily went back to the original value and didn't fall into the electrochemical dead zone. The absence of complete microstructure collapse prevented the permanent downfall of OCV, taking advantage of the extremely dense microstructure.

4. Conclusion

A new way to characterize a charge transfer reaction of solid oxide fuel cells was introduced and demonstrated successfully. Patterned Pt electrode with limited reaction sites was realized by introducing the patterned electrode geometry. The electrochemical behavior of the cells was successfully controlled by manipulating the number of patterned strips. The ratio of faradaic impedances of each cell is exactly consistent with the ratio of TPB density. It was demonstrated that the control of reaction domains is able to be realized. The dense microstructure of Pt cathode also helped the cell voltage to stay at adequate OCV value for 10 h of operation at 500 °C. However, delamination of Pt was found as well, which changed EIS Nyquist plot charge transfer impedance. This new approach to analyzing the electrode-electrolyte interaction is expected to give a breakthrough to quantitatively and qualitatively investigate materials behavior over fuel cells operation without messy deliberation for a structural variable.

Acknowledgements

This work was supported by the National Research Foundation under the Ministry of Science, ICT and Future Planning of Korea (NRF-2017R1C1B5018183, 2017M3D1A1040688, 2018H1D3A2000661). Also, this work was supported by the Global Frontier R&D Program on Center for Multiscale Energy System funded by the National Research Foundation (NRF) under the Ministry of Science, ICT & Future Planning, Korea (2012M3A6A7054855).

References

[1] R. O'Hayre, S.-W. Cha, W. Colella, F.B. Prinz, Fuel Cell Fundamentals, John Wiley & Sons, Inc., Hoboken, NJ, USA, 2016, https://doi.org/10.1002/9781119191766.
[2] R. O'Hayre, D.M. Barnett, F.B. Prinz, The triple phase boundary, J. Electrochem. Soc. 152 (2005) A439, https://doi.org/10.1149/1.1851054.
[3] M. Brown, S. Primdahl, M. Mogensen, Structure/performance relations for Ni/Yttria-stabilized zirconia anodes for solid oxide fuel cells, J. Electrochem. Soc. 147 (2000) 475–485, https://doi.org/10.1149/1.1393220.
[4] T. Wu, W. Zhang, B. Yu, J. Chen, A novel electrolyte-electrode interface structure with directional micro-channel fabricated by freeze casting: a minireview, Int. J. Hydrog. Energy 42 (2017) 29900–29910, https://doi.org/10.1016/j.ijhydene.2017.06.224.
[5] F. Wankmüller, J. Szász, J. Joos, V. Wilde, H. Störmer, D. Gerthsen, E. Ivers-Tiffée, Correlative tomography at the cathode/electrolyte interfaces of solid oxide fuel cells, J. Power Sources 360 (2017) 399–408, https://doi.org/10.1016/j.jpowsour.2017.06.008.
[6] J.A. Cebollero, R. Lahoz, M.A. Laguna-Bercero, A. Larrea, Tailoring the electrode-electrolyte interface of Solid Oxide Fuel Cells (SOFC) by laser micro-patterning to improve their electrochemical performance, J. Power Sources 360 (2017) 336–344, https://doi.org/10.1016/j.jpowsour.2017.05.106.
[7] M. Nagamori, T. Shimonosono, S. Sameshima, Y. Hirata, N. Matsunaga, Y. Sakka, Densification and cell performance of gadolinium-doped ceria (GDC) electrolyte/NiO-GDC anode laminates, J. Am. Ceram. Soc. 92 (2009) 117–121, https://doi.org/10.1111/j.1551-2916.2008.02646.x.
[8] K.-Y. Liu, L. Fan, C.-C. Yu, P.-C. Su, Thermal stability and performance enhancement of nano-porous platinum cathode in solid oxide fuel cells by nanoscale ZrO_2 capping, Electrochem. Commun. 56 (2015) 65–69, https://doi.org/10.1016/j.elecom.2015.04.008.
[9] H.-S. Noh, J. Hong, H. Kim, K.J. Yoon, B.-K. Kim, H.-W. Lee, J.-H. Lee, J.-W. Son, Scale-up of thin-film deposition-based solid oxide fuel cell by sputtering, a commercially viable thin-film technology, J. Electrochem. Soc. 163 (2016) F613–F617, https://doi.org/10.1149/2.0331607jes.
[10] I. Chang, S. Woo, M.H. Lee, J.H. Shim, Y. Piao, S.W. Cha, Characterization of porous Pt films deposited via sputtering, Appl. Surf. Sci. 282 (2013) 463–466, https://doi.org/10.1016/j.apsusc.2013.05.153.
[11] I. Chang, S. Ji, J. Park, M.H. Lee, S.W. Cha, Ultrathin YSZ coating on Pt cathode for high thermal stability and enhanced oxygen reduction reaction activity, Adv. Energy Mater. 5 (2015) 1402251, , https://doi.org/10.1002/aenm.201402251.
[12] J. Park, Y. Lee, I. Chang, W. Lee, S.W. Cha, Engineering of the electrode structure of thin film solid oxide fuel cells, Thin Solid Films 584 (2015) 125–129, https://doi.org/10.1016/j.tsf.2014.11.018.
[13] P.C. Su, C.C. Chao, J.H. Shim, R. Fasching, F.B. Prinz, Solid oxide fuel cell with corrugated thin film electrolyte, Nano Lett. 8 (2008) 2289–2292, https://doi.org/10.1021/nl800977z.
[14] J. An, Y.-B. Kim, J. Park, T.M. Gür, F.B. Prinz, Three-dimensional nanostructured bilayer solid oxide fuel cell with 1.3 W/cm^2 at 450 °C, Nano Lett. 13 (2013) 4551–4555, https://doi.org/10.1021/nl402661p.
[15] D. Ding, X. Li, S.Y. Lai, K. Gerdes, M. Liu, Enhancing SOFC cathode performance by surface modification through infiltration, Energy Environ. Sci. 7 (2014) 552, https://doi.org/10.1039/c3ee42926a.
[16] D. Han, J. Liu, Y.B. He, H.F. Wang, X.Z. Zhang, S.R. Wang, Fabrication of a quasi-symmetrical solid oxide fuel cell using a modified tape casting/screen-printing/infiltrating combined technique, Int. J. Hydrog. Energy 43 (2018) 960–967, https://doi.org/10.1016/j.ijhydene.2017.11.082.
[17] A.S. Mehranjani, D.J. Cumming, D.C. Sinclair, R.H. Rothman, Low-temperature co-sintering for fabrication of zirconia/ceria bi-layer electrolyte via tape casting using a Fe_2O_3 sintering aid, J. Eur. Ceram. Soc. 37 (2017) 3981–3993, https://doi.org/10.1016/j.jeurceramsoc.2017.05.018.
[18] A. Bieberle, L.P. Meier, L.J. Gauckler, The electrochemistry of Ni pattern anodes used as solid oxide fuel cell model electrodes, J. Electrochem. Soc. 148 (2001) A646, https://doi.org/10.1149/1.1372219.
[19] Y.B. Kim, C.-M. Hsu, S.T. Connor, T.M. Gür, Y. Cui, F.B. Prinz, Nanopore patterned Pt Array electrodes for triple phase boundary study in low temperature SOFC, J. Electrochem. Soc. 157 (2010) B1269, , https://doi.org/10.1149/1.3455046.
[20] W.C. Chueh, Y. Hao, W. Jung, S.M. Haile, High electrochemical activity of the oxide phase in model ceria-Pt and ceria-Ni composite anodes, Nat. Mater. 11 (2012) 155–161, https://doi.org/10.1038/nmat3184.
[21] K.M. Subramaniam, L.L. Rajeswara Rao, N. Jampana, Inductively coupled reactive ion etching studies on sputtered yttria stabilized zirconia thin films in SF6, Cl2, and BCl3 chemistries, J. Vac. Sci. Technol. B 33 (2015) 022003, , https://doi.org/10.1116/1.4907707.
[22] I.W. Rangelow, Critical tasks in high aspect ratio silicon dry etching for micro-electromechanical systems, J. Vac. Sci. Technol. A 21 (2003) 1550–1562, https://doi.org/10.1116/1.1580488.
[23] J.L. Bosse, B.D. Huey, Error-corrected AFM: a simple and broadly applicable approach for substantially improving AFM image accuracy, Nanotechnology 25 (2014), https://doi.org/10.1088/0957-4484/25/15/155704.
[24] C.H. Chang, M.H. Kryder, Effect of substrate roughness on microstructure, uniaxial anisotropy, and coercivity of Co/Pt multilayer thin films, J. Appl. Phys. 75 (1994) 6864–6866, https://doi.org/10.1063/1.356810.
[25] E. Slavcheva, G. Ganske, G. Topalov, W. Mokwa, U. Schnakenberg, Effect of sputtering parameters on surface morphology and catalytic efficiency of thin platinum films, Appl. Surf. Sci. 255 (2009) 6479–6486, https://doi.org/10.1016/j.apsusc.2009.02.033.

[26] B. Okolo, P. Lamparter, U. Welzel, T. Wagner, E.J. Mittemeijer, The effect of deposition parameters and substrate surface condition on texture, morphology and stress in magnetron-sputter-deposited Cu thin films, Thin Solid Films 474 (2005) 50–63, https://doi.org/10.1016/j.tsf.2004.08.006.
[27] J. Liu, F. Ciucci, Modeling the impedance spectra of mixed conducting thin films with exposed and embedded current collectors, Phys. Chem. Chem. Phys. 19 (2017) 26310–26321, https://doi.org/10.1039/c7cp03703a.
[28] Y.H. Lee, G.Y. Cho, I. Chang, S. Ji, Y.B. Kim, S.W. Cha, Platinum-based nanocomposite electrodes for low-temperature solid oxide fuel cells with extended lifetime, J. Power Sources 307 (2016) 289–296, https://doi.org/10.1016/j.jpowsour.2015.12.089.